A Phase-Shifting MPPT to Mitigate Interharmonics from Cascaded H-Bridge PV Inverters

Pan, Y.; Sangwongwanich, A.; Yang, Y.; Blaabjerg, F.

Published in:
IEEE Transactions on Industry Applications

DOI (link to publication from Publisher):
10.1109/TIA.2020.3000969

Publication date:
2021

Document Version
Accepted author manuscript, peer reviewed version

A Phase-Shifting MPPT to Mitigate Interharmonics from Cascaded H-Bridge PV Inverters

Yiwei Pan, *Student Member, IEEE*, Ariya Sangwongwanich, *Member, IEEE*, Yongheng Yang, *Senior Member, IEEE*, and Frede Blaabjerg, *Fellow, IEEE*

***Abstract*—Interhamonics are an emerging issue in photovoltaic (PV) systems. It has been revealed in previous studies that the maximum power point tracking (MPPT) control is one cause for interharmonics. In cascaded H-bridge (CHB) PV inverters, if the MPPT perturbations of the CHB cells are in-phase, the sum of the voltages of all CHB cells will oscillate with a higher amplitude, leading to large interharmonics in the grid. To address this issue, a phase-shifting MPPT (PS-MPPT) method is thus proposed in this paper. By properly shifting the phase-angle of the MPPT perturbation of each CHB cell, the oscillation of the equivalent total DC voltage can be effectively mitigated, and in turn, the interharmonics can be suppressed to a large extent. The proposed PS-MPPT scheme has been demonstrated on a 3-cell and 4-cell CHB PV inverters in simulations and a 2-cell experimental setup, and the implementation in *n*-cell CHB PV inverters has further been discussed. A hybrid PS-MPPT method is also developed further to improve the interharmonic mitigation performance. Simulation and experimental results have validated the effectiveness of the proposed method in terms of interharmonic suppression.**

***Index Terms*—Cascaded H-bridge (CHB), harmonics, interharmonics, maximum power point tracking (MPPT), photovoltaic (PV) systems.**

I. Introduction

With the increasing installation of PV systems, challenging issues related to power quality are emerging [1]. For example, interharmonics have become critical recently due to the large-scale adoption of power electronics [2]-[9]. As observed in laboratory tests [2], [3] and field measurements [4], [5], PV inverters potentially contribute to interharmonics, which may adversely cause voltage fluctuation, flickering and unintentional disconnection [6]. Therefore, as recommended by the International Electrotechnical Commission Technical Specifications (IEC TS) 63102 [7], interharmonics are considered as one of the assessment criteria for grid-connected PV systems. In the literature, it has been revealed that the MPPT perturbation can lead to interharmonics [2]-[6]. As shown in Fig. 1, experimental tests on a 3-kW single-phase grid-connected PV system have provided solid evidence of this mechanism. It is further explained as follows: the low-frequency oscillation due to the MPPT will interact with the grid fundamental frequency through the control, and subsequently, interharmonics are then generated [2].

Manuscript received March 11, 2020; accepted June 2, 2020. This work was supported by the research project – Reliable Power Electronic based Power Systems (REPEPS) by THE VELUX FOUNDATIONS under Award Ref. No.: 00016591. *(Corresponding Author: Yongheng Yang.)*

The authors are with the Department of Energy Technology, Aalborg University, Aalborg 9220, Denmark (e-mail: ypa@et.aau.dk; ars@et.aau.dk; yoy@et.aau.dk; fbl@et.aau.dk).

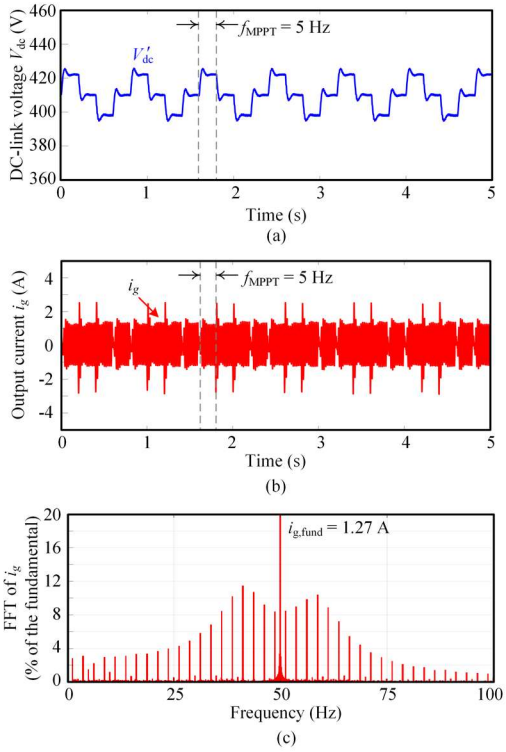

Fig. 1. Experimental results of a 3-kW single-stage PV inverter operating at 10% of the rated power with a Perturb and Observe (P&O) MPPT control (the MPPT sampling rate f_{MPPT} = 5 Hz, the perturbation step-size v_{step} = 12 V, and $i_{g,fund}$ denotes the fundamental component of the grid current) [2]: (a) DC-link voltage where the double-line frequency components have been filtered out, (b) grid current, and (c) fast Fourier transform (FFT) analysis of the grid current.

In the literature, many attempts have been made to alleviate the interharmonics from single-phase full-bridge PV inverters. As suggested in [2], the sampling rate of the MPPT algorithm can be reduced. However, this leads to slow MPPT dynamics, which may eventually reduce the PV energy yield. In [8], an adaptive gain method and a rate limiter method have been proposed. With the two methods, interharmonics can be suppressed by limiting the abrupt change in the grid current, but the suppression performances are limited, where only a certain range of interharmonic frequencies (e.g., high-order) can be suppressed. In [6], a random sampling rate MPPT method was proposed. By avoiding the periodic disturbance in the grid current, dominant interharmonics can be mitigated to a large extent. Nevertheless, its mitigation capability is limited, since the power oscillation of the MPPT remains, which is the main source of interharmonics. Nevertheless, previous researches were mainly focused on the interharmonic mitigation of one single unit. For applications with larger power capacities or

higher EMI requirements, multi-level inverters can be employed in PV systems. However, since the PV panels can be integrated into multi-level inverters in many different configurations [9]-[11], the interharmonic issue in the multi-level-topology-based PV inverter is more complex than one single unit.

Among the multilevel topologies, the cascaded H-bridge (CHB) configuration has been the most attractive one due to its modularity, high efficiency, and simple layout [10]-[15]. The overall diagram of the CHB PV inverter is shown in Fig. 2. According to the prior-art exploration, the MPPT perturbation for each CHB will inevitably generate interharmonics. If the DC-side oscillations of CHB cells are in-phase, the total DC voltage oscillation (which is the sum of all the CHB cell voltages) will be magnified. As a result, the interharmonics emission in the CHB PV inverter can be much severer than one single inverter. However, seen from the entire system perspective, there might be more possibilities to address the interharmonics, e.g., through coordinated control of the CHB cells. For instance, in [16], a DC-link ripple feed-forward compensation method has been introduced to reject low-order harmonics. Nevertheless, the feed-forward method is not capable to suppress interharmonics caused by the MPPT control.

As aforementioned, the distributed DC-side of the CHB topology offers more control flexibility for the MPPT, which can potentially improve the interharmonic mitigation. Accordingly, a phase-shifting MPPT (PS-MPPT) scheme to mitigate the interharmonics for the CHB PV systems is proposed in this paper, which is an extension of the conference paper [17]. More specifically, by properly adjusting the phase-shift between the MPPT perturbation of each CHB cell, the power oscillation at the DC-side can be minimized, and thereby, suppressing the interharmonics. However, the PS-MPPT scheme cannot fully eliminate the oscillation when an odd number of cells are cascaded. To overcome this, a hybrid PS-MPPT scheme is further developed to enhance the interharmonic suppression performance for the odd number cases. The rest of this paper is organized as follows. In Section II, the two-layer control structure of the CHB PV inverter is briefly introduced, as well as the particular interharmonic magnification issue in the CHB PV inverter. Then, the proposed PS-MPPT scheme is discussed in detail in Section III. In Section IV, the effectiveness of the proposed method in terms of interharmonic mitigation is verified by simulations and experiments on a single-phase CHB PV inverter. Moreover, for *n*-cell CHB PV inverters (*n* indicates the number of cells), the implementation and control have been further elaborated considering practical conditions. Finally, concluding remarks are provided in Section V.

II. System Description and Interharmonics

A. Control Structure

The CHB-PV inverter is shown in Fig. 2, where the control is achieved with a two-layer structure, as shown in Fig. 3, which can be easily achieved in both centralized and decentralized control systems [11], [15]. For the decentralized control, the primary control obtains the equivalent total DC voltage V'_{total} and voltage reference for the k^{th} cell V^*_{PVk} (k denotes the index of CHB cells) from all the secondary controllers through low-bandwidth communication (LBC). The primary control also

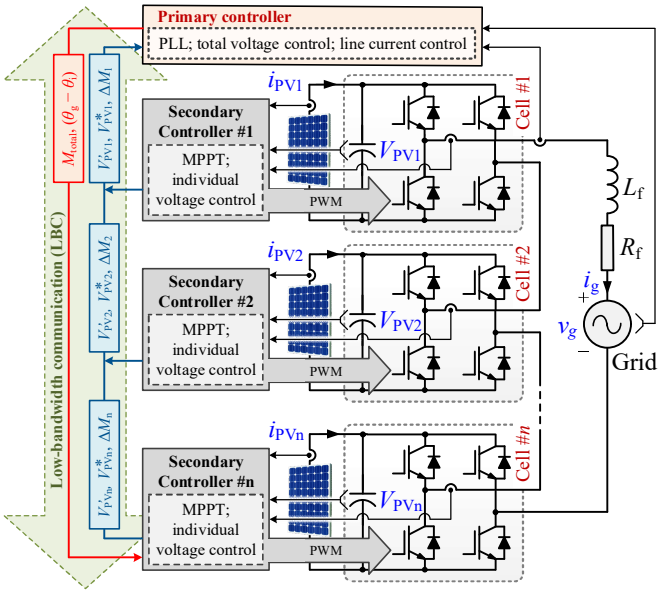

Fig. 2. Overall control diagram of a single-phase grid-connected CHB PV inverter (PLL – phase locked loop; MPPT – maximum power point tracking), where i_{PVk} and V_{PVk} (k = 1, 2, ..., n) represent the corresponding current and voltage of the k^{th} cell, L_{f} and R_{f} indicate the output AC filter impedance, and i_{g} is the grid current.

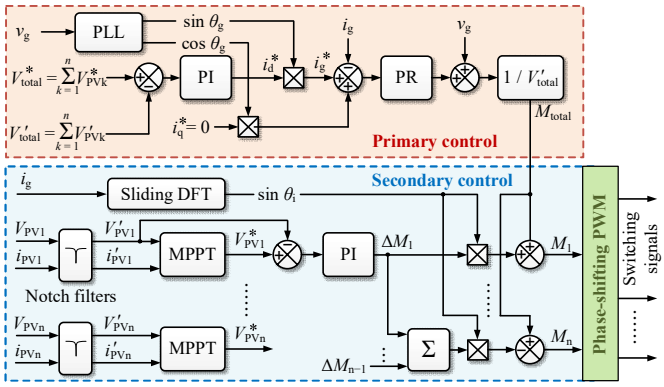

Fig. 3. Control diagram of a single-phase CHB PV inverter (DFT - discrete Fourier transform; PWM - pulse width modulation; PI - proportional integral; PR - proportional resonant), where M_{k} indicates the corresponding modulation index of the k^{th} H-bridge cell and M_{total} is the equivalent total modulation index.

regulates the total DC voltage V'_{total} according to the sum of the MPPT voltage references V^*_{total} through a voltage proportional-integral (PI) regulator, which generates the amplitude of the current reference i^*_{d}. The grid current reference i^*_{g} can then be obtained by taking the grid phase θ_{g} (e.g., from a phase-locked loop - PLL) into the account, as shown in Fig. 3. Then, the grid current i_{g} is regulated according to the current reference by a proportional resonant (PR) controller, giving the modulation index M_{total}, which is equally distributed to each CHB cell. The secondary control is responsible for the individual MPPT control, which is achieved by regulating the corresponding PV voltage. As shown in Fig. 3, the individual PV voltage reference V^*_{PVk} is generated by each MPPT controller. In this paper, the Perturb and Observe (P&O) MPPT algorithm is employed. The DC voltage of each CHB cell is then regulated according to the

voltage reference V^*_{PVk} through a PI controller. The modulation index for the k^{th} CHB cell can be calculated as

$$M_{\mathrm{k}} = M_{\mathrm{total}} + \Delta M_{\mathrm{k}} \sin\theta_{\mathrm{i}} \tag{1}$$

where θ_{i} is the phase-angle of the line current i_{g} that is extracted through a sliding discrete Fourier transform (SDFT) method [15], [18]. For the last CHB cell (i.e., the n^{th} cell), the modulation index can be given as

$$M_{\mathrm{n}} = M_{\mathrm{total}} - \left(\sum_{k=1}^{n-1} \Delta M_{\mathrm{k}}\right) \sin\theta_{\mathrm{i}} \tag{2}$$

Moreover, the LBC-based PWM synchronization method in [19] or the line-current-based PWM synchronization method in [14] can be adopted, which can give a high-quality multilevel output voltage and current in the decentralized manner. Therefore, with the above-mentioned two-layer control method, the module-level MPPT can be achieved for the CHB inverter, enabling to harvest more energy [11], [12].

B. Interharmonics

When the P&O MPPT is employed, in steady-state, the DC voltage of the PV panel oscillates around the maximum power point (MPP) at a frequency of f_{MPPT} / 4 with f_{MPPT} being the MPPT frequency of one converter cell [9]. The oscillation has three levels, in this case, if the fundamental components of the DC voltage oscillations of all cells are in-phase, the oscillation amplitude of the equivalent total DC voltage will be n times larger than the P&O perturbation step-size of the individual CHB cell. To demonstrate this, a steady-state operation of a 4-cell CHB PV inverter is shown in Fig. 4, where the MPPT perturbations of all CHB cells are in-phase. As shown in Fig. 4, the equivalent total DC voltage oscillates with an amplitude, which is 4 times larger than the oscillation on one CHB cell (v_{step}). This amplified oscillation will consequently lead to larger interharmonics in the grid current, and thus, more efforts should be made to address this issue for high-performance grid-friendly PV systems.

III. Proposed Phase-Shifting MPPT Control

The principle of the proposed PS-MPPT control is to properly adjust (i.e., shift) the phase-angle of each DC voltage reference for the MPPT control in a way to minimize the overall oscillation of the equivalent total DC voltage. Assuming that the same kind of PV converters are cascaded, and the MPPT frequency f_{MPPT} and perturbation step-size v_{step} for all cells are the same, the phase-shifting will make the oscillations on the CHB cell voltages be canceled out. The proposed method is further elaborated on a 4-cell CHB inverter, as shown in Fig. 5. As shown in Fig. 5, if the fundamental component of the voltage reference for the k^{th} converter is shifted by $(k-1)(\pi/2)$ with $k = 1, 2, 3, 4$, there will be no oscillations on the total equivalent voltage reference. Thus, interharmonics can be suppressed due to the elimination of MPPT perturbations in the primary control loops.

To achieve the phase-shifting, firstly, the phase-angle of the fundamental component of the DC voltage oscillation on the individual CHB cell voltage, denoted as φ_{k}, should be extracted. This can be obtained through the SDFT algorithm [18], which features a simple structure for digital implementation with a sliding window and several addition and multiplication operations. The SDFT algorithm to extract the fundamental component of the oscillation due to the MPPT control can be expressed as

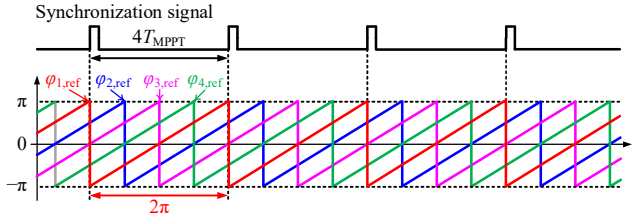

Fig. 6. Generation of phase-angle references $\varphi_{1\text{–}4,\mathrm{ref}}$.

$$A_{\mathrm{fund}}(x+1) = e^{\frac{j\cdot 2\pi\cdot f_{\mathrm{fund}}}{N_{\mathrm{SDFT}}}} \left[A_{\mathrm{fund}}(x) + V^*_{\mathrm{PVk}}(x+N) - V^*_{\mathrm{PVk}}(x)\right] \tag{3}$$

where f_{fund} is the fundamental frequency of the SDFT, with $f_{\mathrm{fund}} = f_{\mathrm{MPPT}}/4$ and N_{SDFT} is the length of the SDFT sampling window. Due to the slow dynamics of the MPPT, a low N_{SDFT} is sufficient, e.g., $N_{\mathrm{SDFT}} = 80$. In addition, in (3), $A_{\mathrm{fund}}(x+1)$ and $A_{\mathrm{fund}}(x)$ are the calculated frequency components for the $(x+1)^{\mathrm{th}}$ and the x^{th} Fourier transform, $V^*_{\mathrm{PVk}}(x+N)$ is the latest sampled voltage reference, and $V^*_{\mathrm{PVk}}(x)$ is the voltage reference recorded N sample-cycles ago. With above, the phase-angle of the DC voltage oscillation for the k^{th} cell can be obtained as

$$\varphi_{\mathrm{k}} = \arctan\left(\frac{\mathrm{Im}\left(A_{\mathrm{fund}}(x+1)\right)}{\mathrm{Re}\left(A_{\mathrm{fund}}(x+1)\right)}\right) \tag{4}$$

in which "Im" and "Re" denote the imaginary and real part of the frequency component.

To synchronize the extracted phase-angles $\varphi_{1\text{-}4}$, a set of shifted phase-angle references are generated with a period of $4/f_{\mathrm{MPPT}}$, as shown in Fig. 6. A positive pulse is generated every $4T_{\mathrm{MPPT}}$ (T_{MPPT} is the MPPT period, and $T_{\mathrm{MPPT}} = 1/f_{\mathrm{MPPT}}$) as a synchronization clock for all phase-angle references. This synchronization signal can be generated in the central controller or in any one of the local controllers, and sent out to all the cells through the serial communication system [19]. When the rise-edge of the synchronization signal is received by each cell, the initial phase-angle of the phase-angle reference is forced to be loaded. In this way, the phase-angle references can be synchronized with a fixed phase-shifting angle between each other.

With these phase-shifted phase-angle references and extracted phase-angles, the phase-angle difference between the reference and the measurement can be calculated by

$$\Delta\varphi_{\mathrm{k}} = \varphi_{\mathrm{k,ref}} - \varphi_{\mathrm{k}} \tag{5}$$

which indicates that $\Delta\varphi_{\mathrm{k}}$ should be controlled as 0 to keep φ_{k} consistent with the phase-angle reference. This can be done by inserting a time delay to the three-stair voltage. For instance, as shown in Fig. 7, before enabling the PS-MPPT control, there are four possible oscillation cases for the first cell with different phase-angles, i.e., $\Delta\varphi_1 = -\frac{1}{2}\pi$, π, $\frac{1}{2}\pi$ and 0. After enabling the phase-shifting control, four types of time delays are correspondingly inserted in each case, i.e., T_{MPPT}, $2T_{\mathrm{MPPT}}$, $3T_{\mathrm{MPPT}}$ and 0. In this way, in steady state, $\Delta\varphi_1$ can be controlled as 0, and the phase-angle of the voltage oscillation on each cell can be synchronized with the phase reference.

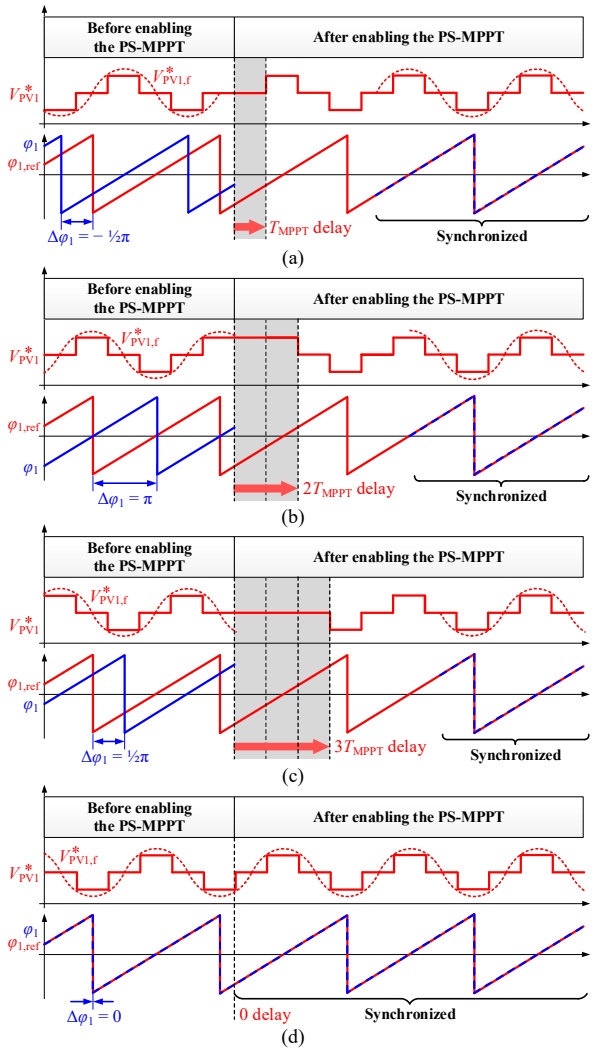

Fig. 7. The operation process of the PS-MPPT for the first cell when the phase-angle difference (a) $\Delta\varphi_1 = -\frac{1}{2}\pi$, (b) $\Delta\varphi_1 = \pi$, (c) $\Delta\varphi_1 = \frac{1}{2}\pi$, and (d) $\Delta\varphi_1 = 0$.

The flowchart of the PS-MPPT method for the first cell is shown in Fig. 8. As it can be observed in Fig. 8, after the start of the MPPT, if the inserted time delay T_{delay} is not zero, T_{delay} will be decreased by T_{MPPT}, and then the MPPT will be terminated for this MPPT cycle. Only when $T_{delay} = 0$ will the conventional MPPT algorithm be executed. Subsequently, if the difference between the maximum and minimum value of $\Delta\varphi_1$ is less than a threshold $\Delta\varphi_{th}$ while the oscillation amplitude $\left|V^*_{PVk,f}\right|$ is larger than a certain threshold $V_{SDFT,th}$ within three consecutive MPPT cycles, the first cell is regarded being operating in the steady state, where its DC voltage reference is a three-stair waveform. In this condition, depending on the value of $\Delta\varphi_1$, four values are assigned to T_{delay}. On the other hand, if $(\Delta\varphi_{1,max} - \Delta\varphi_{1,min})$ is beyond the range of $[-\Delta\varphi_{th}, \Delta\varphi_{th}]$, it is assumed that the first cell is not operating in the three-stair voltage mode (i.e., not the steady-state), and no changes will be made in terms of T_{delay}. In the following MPPT cycles, if T_{delay} is not zero, the conventional MPPT algorithm will still be skipped until T_{delay} reaches zero in the future MPPT cycles. By doing so, the phase-angle of the voltage oscillation can be kept consistent with the phase-angle reference.

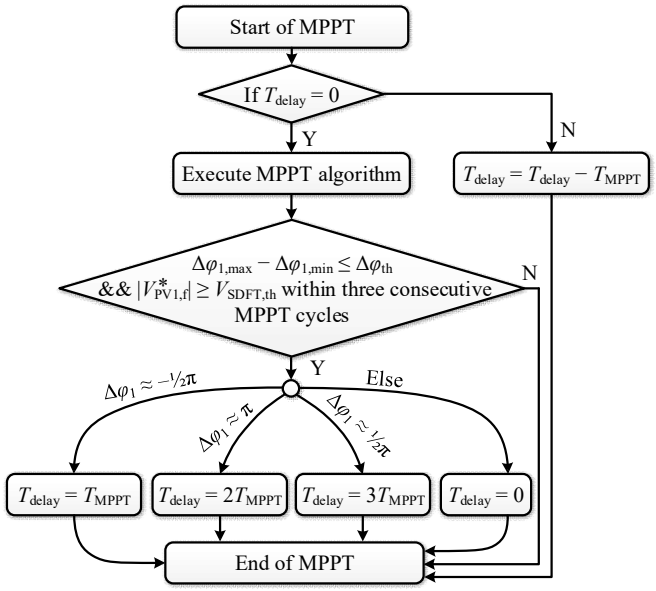

Fig. 8. Flowchart of the phase-shifting MPPT method for the first CHB cell.

IV. PS-MPPT FOR N-CELL CHB PV INVERTERS

In the above discussion, the 4-cell CHB is employed to illustrate the proposed method. For *n*-cell CHB PV inverters, one set of inserted time delays are summarized in Table I. It should be mentioned that when an even number of converter cells are cascaded, the oscillation in the equivalent total voltage can be fully eliminated. However, when the number of cascaded cells is odd, small oscillations (i.e., equivalent to one CHB cell) remains in the equivalent total DC voltage, but the overall interharmonics are reduced significantly. For instance, as shown in Table I, for the 3-cell CHB, the phase-angle references for cell #1, #2 and #3 can be phase-shifted by 0, π/2 and π. In this case, the resultant voltage references are given in Fig. 9(a). As it can be observed from Fig. 9(a), the oscillations of cell #1 and #3 can counteract with each other, while the DC voltage oscillation of cell #2 will inevitably emerge in the equivalent total voltage reference. Even for other phase-shifting values, e.g., 0, 2π/3 and 4π/3 for cell #1, #2 and #3, the oscillation in the equivalent total voltage cannot be completely eliminated, as shown in Fig. 9(b). Nevertheless, comparing to the case where all the oscillating voltages are in-phase, as shown in Fig. 4, the proposed PS-MPPT method is still capable to reduce the oscillation in the equivalent total voltage for the CHB with an odd number of cells. Therefore, with the proposed method, interharmonics in the grid current can be effectively suppressed. When an even number of cells are cascaded, the suppression performance can be better, since the oscillation on the total equivalent voltage reference can be fully eliminated, as illustrated in Fig. 5, where the voltage references for the 4-cell CHB PV inverter are exemplified.

In addition, it can be observed in Table I that the phase-shifting angles are not linearly dispatched for all cells. On the other hand, the phase-shifting angles can also be linearly dispatched within the range of [0, 2π], as shown in Fig. 9(b). For the PS-MPPT scheme with linear-dispatched angles, since the oscillation frequency of the total DC voltage is increased, after the modulation with the fundamental frequency, the

TABLE I
PHASE SHIFT ANGLES OF *N*-CELL CHB PV INVERTERS.

Total number of cells / Cell index	2-cell	3-cell	4-cell	5-cell	6-cell	7-cell
Cell #1	0	0	0	0	0	0
Cell #2	π	π/2	π/2	π/2	π/2	π/2
Cell #3	/	π	π	π	π	π
Cell #4	/	/	3π /2	3π /2	3π /2	3π /2
Cell #5	/	/	/	0	0	0
Cell #6	/	/	/	/	π	π/2
Cell #7	/	/	/	/	/	π

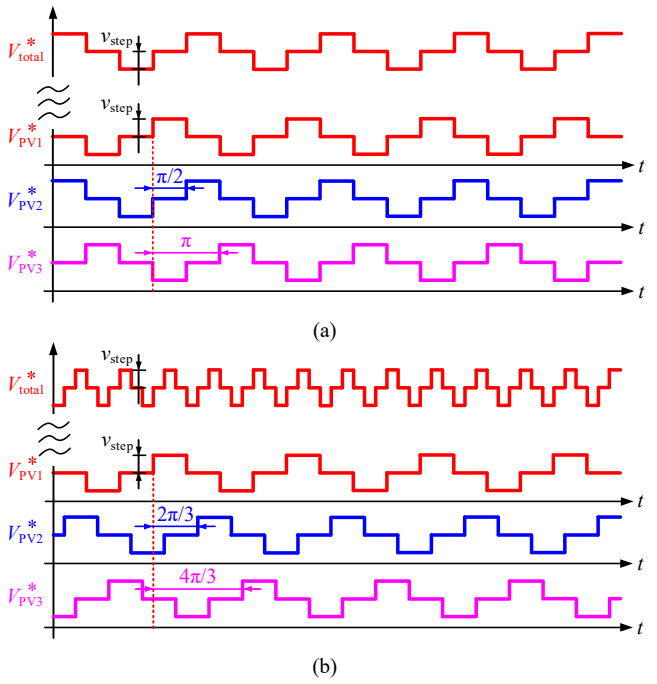

Fig. 9. Voltage references of the 3-cell CHB PV inverter with two sets of phase-shift angles: (a) voltage references for cell #1, #2 and #3 are shifted by 0, π/2 and π, and (b) voltage references for cell #1, #2 and #3 are shifted by 0, 2π/3 and 4π/3.

interharmonics will emerge on fewer frequencies [2]. Thus, both cases are able to suppress the interharmonics. If an even number of cells are cascaded, the performance of these two cases are similar, since the oscillation on the total DC voltage can be eliminated for both cases. If the cascading number is odd, the total DC voltage will oscillate at f_{MPPT} for the non-linear dispatching case, while the frequency will increase to nf_{MPPT} for the linear dispatching case, as examplified in Fig. 9. Obviously, the non-linear dispatching PS-MPPT scheme has a more superior interharmonic performance, owing to that the total DC voltage oscillates at a lower frequency [2]. However, when the cascaded number is high, the dominant interharmonics will become much fewer for the PS-MPPT with linear-dispatched angles, which also lead to a significant interharmonic suppression performance. Therefore, linear dispatched phase-shifting angles can be assigned to individual cells to suppress interharmonics when a high number of cells are cascaded.

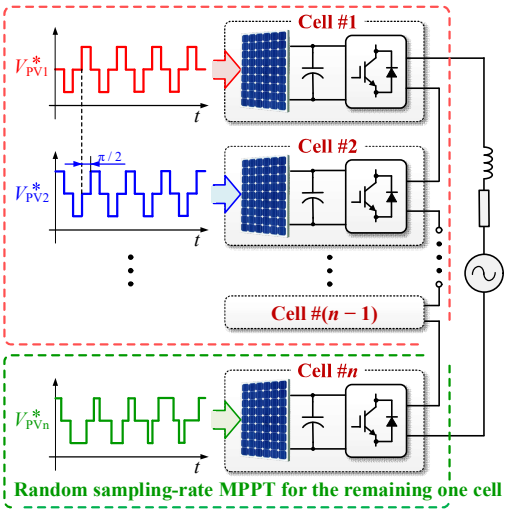

Fig. 10. Demonstration of the hybrid PS-MPPT method.

To enhance the interharmonic suppression performance for the CHB PV inverter with an odd number of cells, a modified hybrid PS-MPPT method can be adopted. It is further explained as follows: the PS-MPPT as discussed in the above is applied to $(n-1)$ cells, so that the oscillations of the $(n-1)$ cells can be canceled out. For the remaining cell, a random-sampling MPPT scheme is adopted. The concept of the hybrid MPPT method is demonstrated in Fig. 10. In this way, the oscillation on the equivalent total DC voltage will be the same as one converter cell with the random-sampling MPPT. Thus, interharmonics can be further suppressed for CHB PV inverters with an odd number of cells.

Nevertheless, unlike the phase-shifting modulation methods in multi-converter systems, where the grid voltage or line current can be employed to achieve synchronization [14], [20], [21], the proposed PS-MPPT highly relies on the LBC to obtain the phase-angle information of the DC voltage oscillations for all converters. Since the communication burden will increase along with the cell number for multi-converter systems [15], many efforts have been made to reduce the dependency on communication for the cascaded converters. In [22]-[24], several communication-free decentralized control schemes were introduced for the grid-connected CHB inverters. Nevertheless, in order to employ the PS-MPPT method for the CHB PV inverters with the communication-free control, the LBC system should be additionally equipped, which will increase the cost of the system. When the cell number is low, the PS-MPPT can still be considered. However, when the cell number is high, the PS-MPPT may not be a cost-effective solution in practice. In this case, randomly selecting the sampling rates for all converter cells seems more reasonable. Due to the randomness of the DC voltage oscillation for each converter, the oscillation on the equivalent total DC voltage will become more arbitrary, leading to the suppression of dominant interharmonics. Although the performance of this method cannot be as good as the PS-MPPT (as the oscillation remains in the equivalent total DC voltage), it can be a cost-effective alternative in the suppression of interharmonics, due to its simplicity in implementation.

Notably, the proposed phase-shifting method is only executed when the MPPT is operating in the steady-state.

TABLE II
PARAMETERS OF THE CHB PV INVERTER.

Rated power for one PV module	214 W
DC link capacitor	680 μF
Grid-side L-filter	5.4 mH
Switching frequency of one cell	5 kHz
Controller sampling frequency	10 kHz
Grid voltage (RMS)	220 V
Grid frequency	50 Hz
MPPT sampling rate	6.67 Hz
MPPT step-size	6 V

During the transient conditions such as the irradiance change, the steady-state criterion in Fig. 8 ($\Delta\varphi_{1,\max} - \Delta\varphi_{1,\min} \leq \Delta\varphi_{th}$ within three consecutive MPPT periods) will lead to the execution of the conventional MPPT method. That is, the dynamic MPPT performance will not be affected by the proposed method. Notably, the oscillation of each DC voltage may not be properly phase-shifted during the transients. This is acceptable in practice, as the interharmonics are mainly introduced in steady-state, when the equivalent total voltage oscillates with a frequency of $f_{MPPT}/4$.

V. SIMULATION AND EXPERIMENTAL RESULTS

In order to validate the effectiveness of the proposed method, simulations and experiments are performed referring to Figs. 2 and 3.

A. Simulation Results

Simulations are carried out on two CHB PV inverters in MATLAB for an odd and even number of cascading converters (i.e., 3 cells and 4 cells). The simulation results are shown in Figs. 11-20. The parameters of the simulation are shown in Table II, where $\Delta\varphi_{th} = 0.1\pi$, $V_{SDFT,th} = 5$ V, and $N_{SDFT} = 80$. Five cases are considered to demonstrate the performance of the proposed method. The performances of different MPPT methods for n-cell CHB PV inverters are also compared through simulations, and the results are given in Fig. 21.

Case 1: Firstly, a 3-cell CHB PV inverter is demonstrated under a constant ambient condition (100 W/m^2 and 25 °C), as shown in Fig. 11. Five PV modules were connected in series to each converter cell, and the maximum power for each PV string is 1066 W. Before t = 2.5 s, the CHB is operating with the conventional MPPT control. In this case, the MPPT perturbations of all CHB cells are in-phase, as shown in Fig. 11. Accordingly, the equivalent total DC voltage oscillates with an amplitude of 18 V (e.g., three times higher than the individual perturbation step-size). Consequently, the grid current has a high amplitude of oscillations. As shown in Fig. 12(a), inter-harmonics appear in the grid current. The main interharmonics locate at 50 ± (2m+1) · (f_{MPPT}/4) Hz [2], where m = 0, 1, 2…, and the largest interharmonic reaches 0.08 A at 5 Hz. When the proposed PS-MPPT is enabled at t = 2.5 s, the oscillation of the equivalent total voltage V'_{total} is suppressed within 0.3 s (which is the required time for adjusting the phase-shifting). After t = 2.8 s, the amplitude of the oscillation on the equivalent total DC voltage is reduced to 6 V. It can be seen from the individual PV panel voltage in Fig. 11(c) that the MPPT perturbation of cell #2 and #3 are now shifted by T_{MPPT} and $2T_{MPPT}$ with respect to cell #1, respectively. By doing so, the interharmonics of the

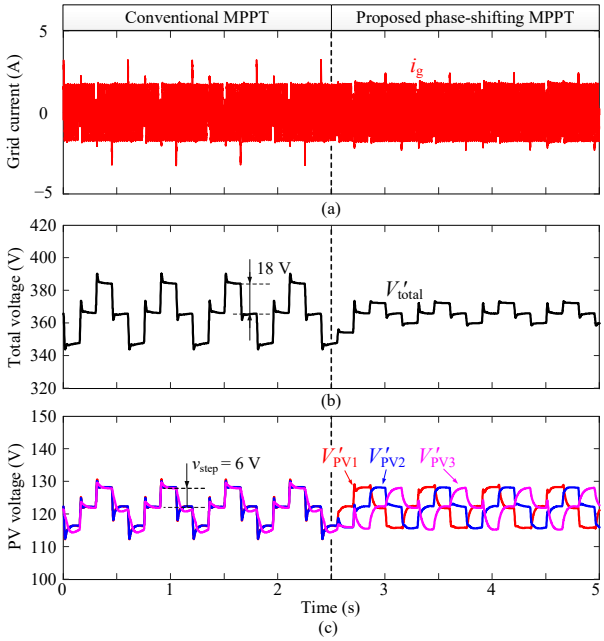

Fig. 11. Simulation results of a 3-cell CHB PV inverter operated at 100 W/m^2 and 25 °C, with the PS-MPPT control enabled at 2.5 s: (a) grid current, (b) filtered equivalent total DC voltage, and (c) filtered PV voltages.

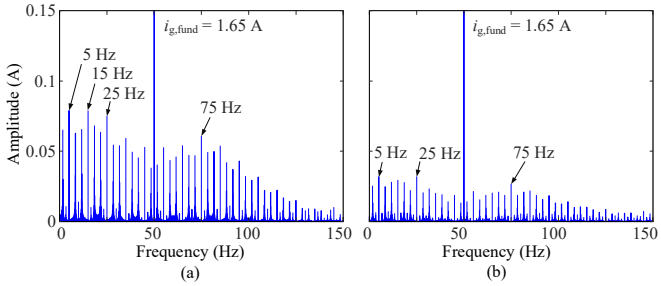

Fig. 12. FFT analysis of the grid current i_g shown in Fig. 11: (a) with the conventional MPPT method and (b) with the proposed PS-MPPT control.

grid current are reduced to approximately one third, with the largest interharmonic being 0.03 A, as shown in Fig. 12(b). Therefore, for the CHB PV inverter with an odd number of cells, the interharmonics in the grid current can be effectively suppressed with the proposed PS-MPPT method.

Case 2: Considering a 4-cell CHB PV inverter under a constant ambient condition (100 W/m^2 and 25 °C), the performance of the proposed method is shown in Fig. 13. In this case, each string has four PV modules in series (total maximum power is 856 W). As it can be observed in Fig. 13, before t = 2.5 s, the oscillation in the equivalent total voltage reaches 24 V, i.e., 4 times larger than the oscillation on one CHB cell, as the reference voltages are in phase. Meanwhile, remarkable interharmonics appear in the grid current, as shown in Fig. 14(a), with the main interharmonics at 50 ± (2k + 1) · (f_{MPPT}/4) Hz, and the largest interharmonic reaches 0.12 A at 5 Hz. When the proposed PS-MPPT method is enabled at t = 2.5 s, the MPPT perturbations of cell #2-4 are shifted by T_{MPPT}, $2T_{MPPT}$ and $3T_{MPPT}$ with respect to cell #1 after 5 MPPT cycles. Compared to Case 1, the oscillation in the equivalent total DC voltage is eliminated in the 4-cell CHB inverter. Thus, the interharmonics are significantly suppressed, as it is shown in Fig. 14(b), where it can be seen that almost all interharmonics

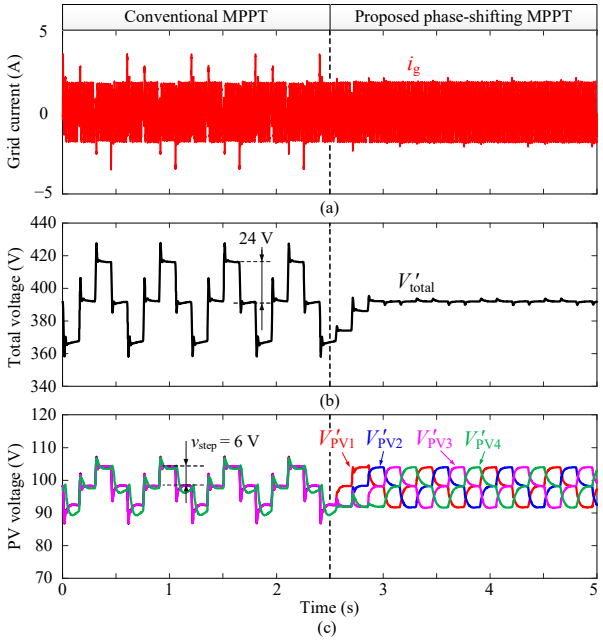

Fig. 13. Simulation results of a 4-cell CHB PV inverter operated at 100 W/m^2 and 25 °C, with the PS-MPPT control enabled at 2.5 s: (a) grid current, (b) filtered equivalent total DC voltage, and (c) filtered PV voltages.

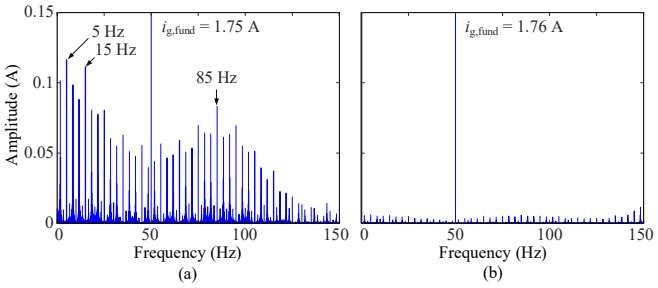

Fig. 14. FFT analysis of the grid current i_g shown in Fig. 13: (a) with the conventional MPPT method and (b) with the proposed PS-MPPT control.

are below 0.01 A. Therefore, for the CHB PV inverters with an even number of cascaded cells, the oscillationin the equivalent total voltage can be effectively suppressed by the proposed PS-MPPT method, resulting in a better interharmonic suppression performance.

Case 3: To verify the performance of the proposed method under irradiance changes, simulations are carried out on the 4-cell CHB PV inverter and the results are provided in Fig. 15. In this case, the irradiance level for PV #1 and PV #3 jumps from 100 W/m^2 to 200 W/m^2 at t = 2 s, the irradiance for PV #2 changes from 100 W/m^2 to 150 W/m^2, and the irradiance for PV #4 changes from 100 W/m^2 to 180 W/m^2 at the same time. As it is seen in Fig. 15, during 2 s to 4 s, PV #1, PV #2, PV #3 and PV #4 approximately enter the steady-state at t = 3.7 s, 3.9 s, 3.6 s and 3.6 s, respectively. During this period, the oscillation can be observed on the equivalent total voltage, as the phase-shift of each cell is being adjusted. After t = 4 s, all the DC voltages are properly phase-shifted, and no oscillations appear in the equivalent total voltage V'_{total}. Consequently, the inter-harmonics are lowered, as shown in Fig. 16.

Case 4: The hybrid PS-MPPT method is further considered for the 3-cell CHB PV inverter with the same conditions in

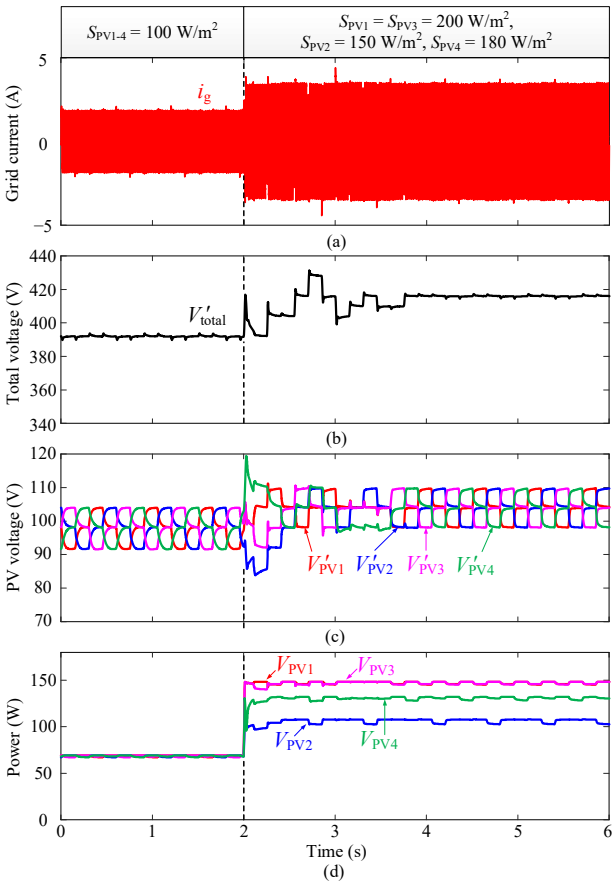

Fig. 15. Performance of the PS-MPPT method under PV irradiance change (S_{PVk} denotes the irradiance for PV #k): (a) grid current, (b) the equivalent total DC voltage, (c) filtered PV voltages, and (d) PV power of 4 CHB cells.

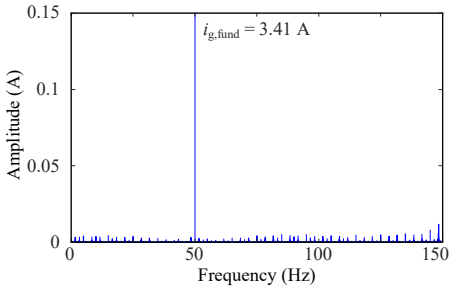

Fig. 16. FFT analysis of the grid current i_g shown in Fig. 15 after t = 4 s.

Case 1. The simulation results are shown in Fig. 17. As shown in Fig. 17, the DC voltage oscillation of cell #3 is phase-shifted by π in respect to cell #1, so that the DC voltage oscillation of the two cells can counteract with each other. At the same time, the MPPT rate for cell #2 is randomly selected between 5 Hz to 20 Hz. Therefore, as shown in Fig. 17, the amplitude of the oscillation on the total equivalent voltage is still 6 V, but the oscillation frequency randomly varies. As a consequence, the interharmonics are distributed to a wider range of frequencies, as shown in Fig. 18, while the amplitudes of interharmonics become much lower compared with the case in Fig. 12(b), with all interharmonics limited below 0.01 A. Therefore, for the CHB PV inverters with an odd number of cells, the hybrid PS-MPPT method can further improve the interharmonic control performance.

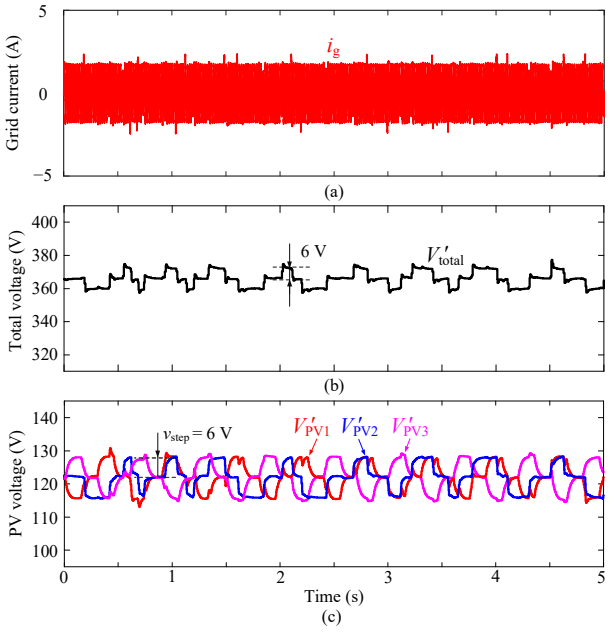

Fig. 17. Performance of the hybrid PS-MPPT method operated at 100 W/m^2 and 25 °C: (a) grid current, (b) the equivalent total DC voltage, and (c) filtered PV voltages.

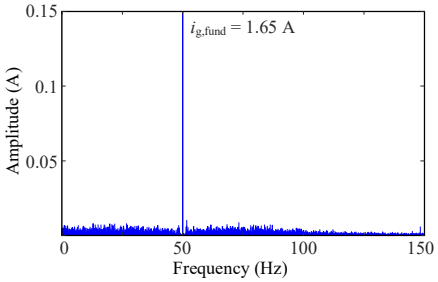

Fig. 18. FFT analysis of the grid current i_g shown in Fig. 17.

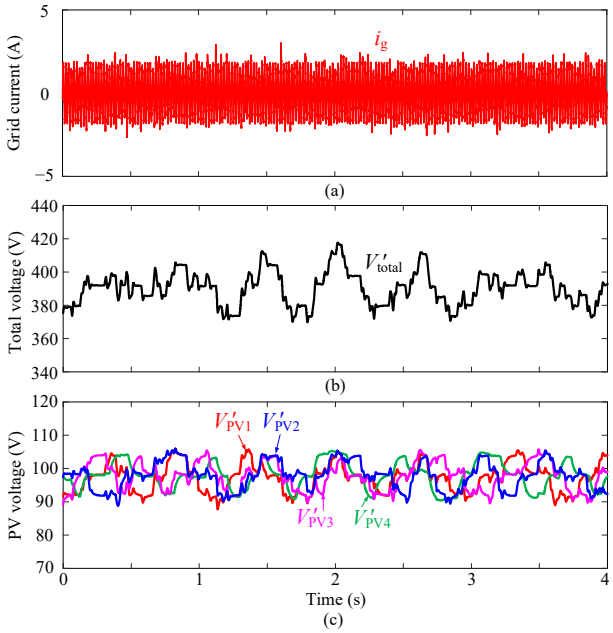

Fig. 19. Performance of the random sampling-rate MPPT method operated at 100 W/m^2 and 25 °C: (a) grid current, (b) the equivalent total DC voltage, and (c) filtered PV voltages.

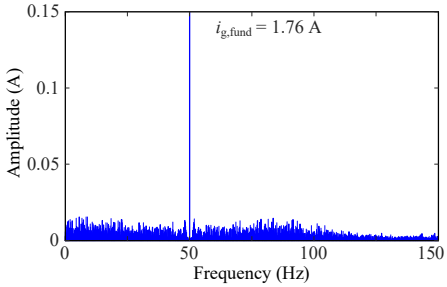

Fig. 20. FFT analysis of the grid current i_g shown in Fig. 19.

Case 5: Similarly, the random sampling-rate MPPT is applied to the 4-cell CHB PV inverter as a comparison. The test conditions are the same with Case 2, and the results are shown in Fig. 19. Due to the random superposition of the frequency-variant DC voltage oscillations of converter cells, the oscillation on the equivalent total DC voltage becomes more arbitrary, as shown in Fig. 19. As a result, all interharmonics are suppressed below 0.02 A, as shown in Fig. 20. Therefore, the random sampling-rate MPPT can mitigate the interharmonics to some extent. Although the performance is not as good as the PS-MPPT in Fig. 14(b), it could still be an alternative owing to its simplicity in implementation, especially for CHB PV inverters with a high number of cascaded cells.

Case 6: To compare the interharmonic performances of the schemes in Section IV for n-cell CHB PV inverters (n varies between 2 to 17), the total interharmonic distortion (TIHD) value explained in [3] is calculated, and the results are shown in Fig. 21. The interharmonic model for the two-level single-phase PV inverter in [2] is adopted in the simulations. The simulation parameters for each cell are the same with Table II, and the operating power for each cell is 311 W. As shown in Fig. 21, with the conventional MPPT, although inter-harmonics will grow higher with more cascaded cells, the TIHD values remain approximately constant at 12.7%. For the random sampling-rate MPPT, the TIHD values are much smaller than the in-phase oscillation case, which become smaller with a large number of cells. The characteristics of the PS-MPPT with linear-dispatched angles and nonlinear-dispatched angles (referring to Table I) are very similar, where the TIHD values for the even-number cases are all below 0.3%, while for the odd-number cases, the PS-MPPT with nonlinear-dispatched angles shows a better performance. Compared with the random sampling-rate MPPT, the PS-MPPT with nonlinear-dispatched angles also performs better. Overall, the TIHD values for all three schemes are very low when the cascaded number is high, e.g., when n = 17, the TIHD values equal to 1.8%, 2.3% and 0.8% for the random sampling-rate, linear-dispatched phase-shifting and nonlinear-dispatched phase-shifting MPPT schemes, respectively. Nevertheless, the performance of the PS-MPPT is further enhanced by the hybrid PS-MPPT, which shows the lowest TIHD values. When n = 17, the TIHD value is only 0.6% for this scheme.

B. Experimental results

To further validate the effectiveness of the proposed method, experiments are also performed on a downscaled 2-cell grid-connected CHB PV inverter, as shown in Fig. 22. A TMS320F28335 digital signal processor was employed to

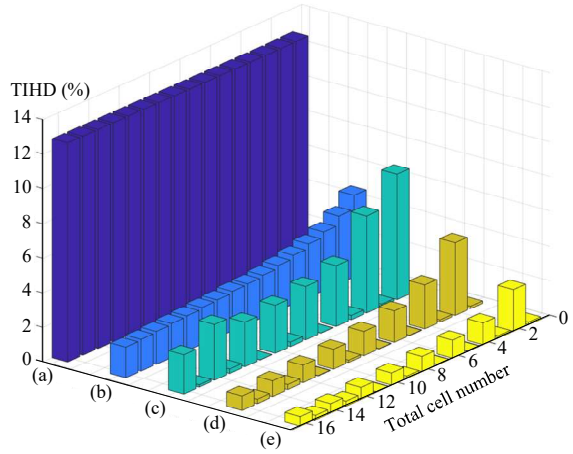

Fig. 21. TIHD values for *n*-cell CHB PV inverters under different MPPT schemes: (a) conventional MPPT, (b) random sampling-rate MPPT, (c) PS-MPPT with linear-dispatched angles, (d) PS-MPPT with nonlinear-dispatched angles (referring to Table I) and (e) hybrid PS-MPPT.

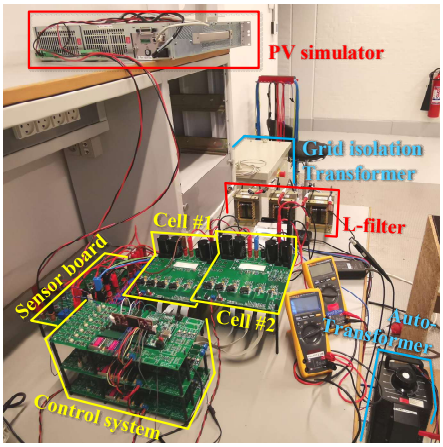

Fig. 22. Photo of the experimental setup of the two-cell CHB PV inverter.

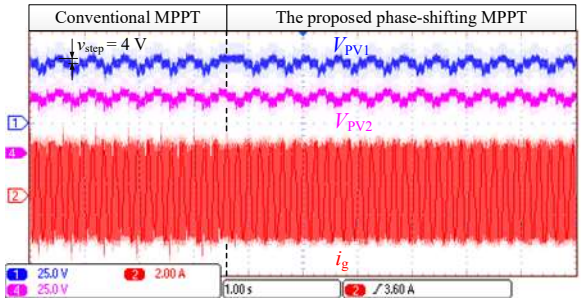

Fig. 23. Experimental results of the PS-MPPT on a 2-cell CHB PV inverter, operated at 200 W/m^2 and 25 °C, with the PV rated power being 300 W for each cell, and the grid voltage is 40 V(rms) (V_{PV1} [25 V/div] and V_{PV2} [25 V/div]: DC voltages for cell #1 and #2; i_g [2 A/div]: grid current).

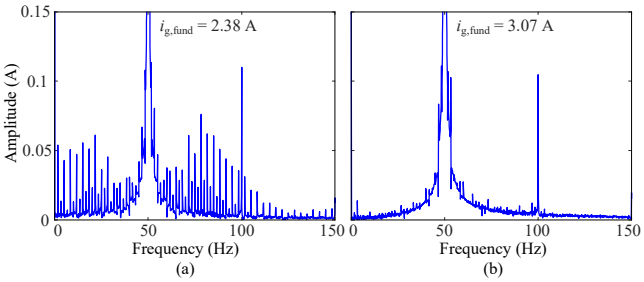

Fig. 24. FFT analysis of the grid current i_g shown in Fig. 23: (a) with in-phase MPPT perturbations and (b) with the proposed PS- MPPT control.

implement the control. Two Infineon FS50R12KT4_B15 IGBT modules were adopted to assemble the 2-cell CHB inverter. One Keysight E4360A PV simulator was used to provide the power supply for two DC buses (i.e., to emulate two separate PV strings). The parameters for the experimental setup are the same as those listed in Table II, except that 1) the rated PV power for each converter cell is 300 W, 2) a 40-V(rms) grid is connected due to the limited output voltage of the PV simulator, and 3) the MPPT step-size v_{step} was reduced to 4 V and $V_{SDFT,th}$ was reduced to 3 V.

Firstly, the effectiveness of the proposed PS-MPPT is verified, and the experimental results are shown in Fig. 23. Before enabling the PS-MPPT, the two DC voltages V_{PV1} and V_{PV2} were oscillating in phase, as observed in Fig. 23. As a consequence, periodical low-frequency spikes appear in the grid current, indicating that there are interharmonics. This is further confirmed in Fig. 24(a), where a large amount of interharmonics can be observed from the frequency spectrum of the grid current, with the dominant interharmonics being around 0.05 A. When the PS-MPPT was enabled, as shown in Fig. 23, the two DC voltages of the CHB inverter were oscillating with an opposite phase-angle after two MPPT cycles, and the grid current became more stable. In this case, the interharmonics were significantly suppressed, as shown in Fig. 24(b). Therefore, with the proposed PS-MPPT, inter-harmonics caused by the in-phase MPPT oscillations of CHB PV inverters can be effectively mitigated.

To demonstrate the dynamics of the PS-MPPT, experiments were performed when the irradiance of PV #1, changes from 200 W/m^2 to 300 W/m^2, and the results are shown in Fig. 25. As shown in Fig. 25, before the irradiance change, the oscillations of V_{PV1} and V_{PV2} were phase-shifted by π with respect to each other. When the irradiance of PV #1 was increased to 300 W/m^2, V_{PV1} was also increased to quickly track the new MPP. At the same time, the 2nd-order ripple on V_{PV1} became higher, indicating that more power was being delivered by cell #1. Then, a time delay of 3 MPPT cycles was inserted for cell #1, and subsequently, the oscillation of V_{PV1} was resynchronized, keeping an opposite phase with V_{PV2}. The frequency spectrum of the steady-state grid current is shown in Fig. 26, which illustrates that interharmonics were effectively suppressed. Therefore, with the proposed PS-MPPT, the MPPT dynamics will not be affected since the PS-MPPT is only effective in steady state.

Since the random sampling-rate MPPT is an effective alternative method for CHB PV inverters with a high number of cells, it was also performed on the 2-cell CHB PV inverter to demonstrate its interharmonic suppression performance. The experimental results are shown in Fig. 27. In this test, the MPPT sampling-rates for both converter cells vary between 5 Hz to 20 Hz. As shown in Fig. 27, the current spikes appear randomly, and the frequency spectrum in Fig. 28 shows that the interharmonics are suppressed compared with the case in Fig. 24(a). In addition, compared with the experimental results in Fig. 24(b), it is also clear that the interharmonic suppression performance for the random-sampling MPPT method is not as

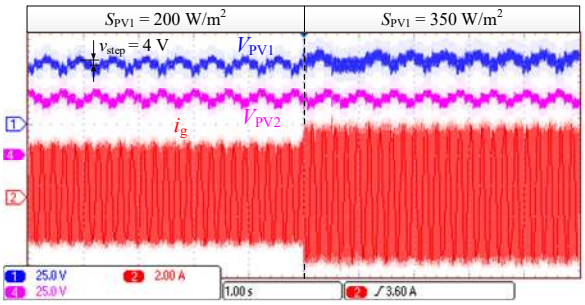

Fig. 25. Experimental results of the PS-MPPT on a 2-cell CHB PV inverter under the irradiance change of PV #1: (V_{PV1} [25 V/div] and V_{PV2} [25 V/div]: DC voltages for cell #1 and #2; i_g [2 A/div]: grid current).

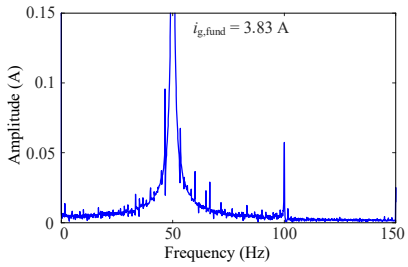

Fig. 26. FFT analysis of the grid current i_g shown in Fig. 25.

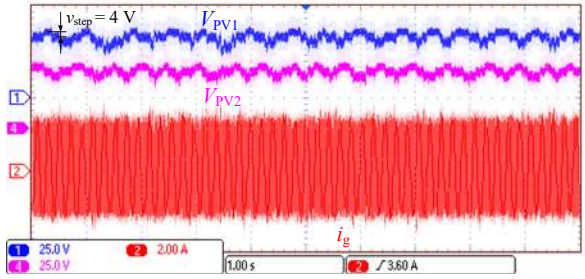

Fig. 27. Experimental results of the random sampling-rate MPPT on a 2-cell CHB PV inverter, operated at 200 W/m² and 25 °C: (V_{PV1} [25 V/div] and V_{PV2} [25 V/div]: DC voltages for cell #1 and #2; i_g [2 A/div]: grid current).

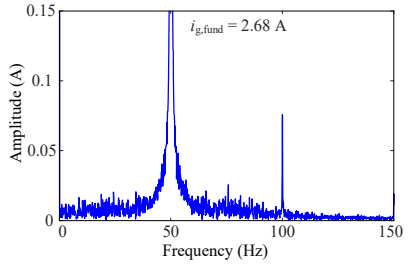

Fig. 28. FFT analysis of the grid current i_g shown in Fig. 27.

good as the PS-MPPT. However, it could still be one practical solution in suppressing interharmonics for applications with a high number of cascaded cells.

VI. Conclusions

In the CHB PV inverter, the oscillation in the equivalent total voltage may be amplified, if the MPPT perturbations of all CHB cells are in-phase. This can lead to larger inter-harmonics in the grid current when the conventional MPPT control is employed. To tackle this issue, a PS-MPPT method for the CHB PV inverter has been proposed in this paper. The proposed method shifts the phase of the MPPT perturbation of each CHB cell in a way to counteract with each other. By doing so, the oscillation of the equivalent total voltage can be suppressed, and the interharmonics can be significantly reduced, while maintaining the MPPT performance. This method is simple for implementation, and can be easily expanded to *n*-cell CHB PV inverters. When an even number of cells are cascaded, the proposed method can almost fully eliminate the interharmonics. When an odd number of cells are cascaded, the hybrid PS-MPPT method proposed in this paper can be adopted to maintain the interharmonic suppression performance. Moreover, when the number is high, the random sampling-rate MPPT method can also be a cost-effective way to mitigate interharmonics.

References

[1] *IEEE Standard for Interconnection and Interoperability of Distributed Energy Resources with Associated Electric Power Systems Interfaces*, IEEE Standard 1547-2018, Apr. 2018.

[2] A. Sangwongwanich, Y. Yang, D. Sera, H. Soltani, and F. Blaabjerg, "Analysis and modeling of interharmonics from grid-connected photovoltaic systems," *IEEE Trans. Power Electron.*, vol. 33, no. 10, pp. 8353-8364, Oct. 2018.

[3] R. Langella, A. Testa, J. Meyer, F. Mller, R. Stiegler, and S. Z. Djokic, "Experimental-based evaluation of PV inverter harmonic and interharmonic distortion due to different operating conditions," *IEEE Trans. Instrum. Meas.*, vol. 65, no. 10, pp. 2221–2233, Oct. 2016.

[4] V. Ravindran, S. K. Rönnberg, and M. H. J. Bollen, "Interharmonics in PV systems: a review of analysis and estimation methods; considerations for selection of an apt method," *IET Renew. Power Gener.*, vol. 13, no. 12, pp. 2023-2032, Sept. 2019.

[5] V. Ravindran, T. Busatto, S. K. Ronnberg, J. Meyer, and M. Bollen, "Time-varying interharmonics in different types of grid-tied PV inverter systems," *IEEE Trans. Power Del.*, vol. 35, no. 2, pp. 483-496, Apr. 2020.

[6] A. Sangwongwanich and F. Blaabjerg, "Mitigation of interharmonics in PV systems with maximum power point tracking modification," *IEEE Trans. Power Electron.*, vol. 34, no. 9, pp. 8279-8282, Sept. 2019.

[7] *Grid code compliance assessment methods for grid connection of wind and PV power plants*, Ed. 1, IEC/TS 63102, 2016.

[8] A. Sangwongwanich, Y. Yang, D. Sera, and F. Blaabjerg, "Inter-harmonics from grid-connected PV systems: mechanism and mitigation," in *Proc. 2017 IEEE 3rd Int. Future Energy Electron. Conf. (IFEEC-ECCE Asia)*, Jun. 2017, pp. 722–727.

[9] Y. Yang, K. A. Kim, F. Blaabjerg, and A. Sangwongwanich, *Advances in Grid-Connected Photovoltaic Power Conversion Systems*, Publisher: Woodhead Publishing, 2018.

[10] X. Zhang, T. Zhao, W. Mao, D. Tan, and L. Chang, "Multilevel inverters for grid-connected photovoltaic applications: examining emerging trends," *IEEE Power Electron. Mag.*, vol. 5, no. 4, pp. 32-41, Dec. 2018.

[11] E. Villanueva, P. Correa, J. Rodriguez, and M. Pacas, "Control of a single-phase cascaded H-bridge multilevel inverter for grid-connected photovoltaic systems," *IEEE Trans. Ind. Electron.*, vol. 56, no. 11, pp. 4399-4406, Nov. 2009.

[12] B. Xiao, L. Hang, J. Mei, C. Riley, L. M. Tolbert, and B. Ozpineci, "Modular cascaded H-bridge multilevel PV inverter with distributed MPPT for grid-connected applications," *IEEE Trans. Ind. Appl.*, vol. 51, no. 2, pp. 1722-1731, Mar./Apr. 2015.

[13] A. Lashab, D. Sera, F. Hahn, L. Camurca, Y. Terriche, M. Liserre, and J. M. Guerrero, "Cascaded multilevel PV inverter with improved harmonic performance during power imbalance between power cells," *IEEE Trans. Ind. Appl.* vol. 56, no. 3, pp. 2788-2798, May./Jun. 2020.

[14] L. Du and J. He, "A simple autonomous phase-shifting PWM approach for cascaded H-Bridge converters," *IEEE Trans. Power Electron.*, vol. 34, no. 12, pp. 11516-11520, Dec. 2019.

[15] Y. Pan, C. Zhang, S. Yuan, A. Chen and J. He, "A decentralized control method for series connected PV battery hybrid microgrid," in *Proc. IEEE Transp. Electrific. Conf. Expo, Asia-Pacific (ITEC Asia-Pacific)*, Harbin, China, Aug. 2017, pp. 1–6.

[16] S. Kouro, P. Lezana, M. Angulo and J. Rodriguez, "Multicarrier PWM with DC-link ripple feedforward compensation for multilevel inverters," *IEEE Trans. Power Electron.*, vol. 23, no. 1, pp. 52-59, Jan. 2008.

[17] Y. Pan, A. Sangwongwanich, Y. Yang, and F. Blaabjerg, "A phase-shifting MPPT method to mitigate interharmonics from cascaded H-bridge PV inverters," in *Proc. IEEE APEC Expo*., Mar. 2020, pp. 1-6.
[18] E. Jacobsen and R. Lyons, "The sliding DFT," *IEEE Signal Process. Mag*., vol. 20, no. 2, pp. 74–80, Mar. 2003.
[19] Y. M. Park, J. Y. Yoo, and S. B. Lee. "Practical implementation of PWM synchronization and phase-shift method for cascaded H-bridge multilevel inverters based on a standard serial communication protocol," *IEEE Trans. Ind. Appl*., vol. 44, no. 2, pp. 634-643, Mar./Apr., 2008.
[20] Y. Yang, P. Davari, F. Zare, and F. Blaabjerg, "A DC-link modulation scheme with phase-shifted current control for harmonic cancellations in multidrive applications," *IEEE Trans. Power Electron.*, vol. 31, no. 3, pp. 1837-1840, Mar. 2016.
[21] Y. Yang, P. Davari, F. Blaabjerg, and F. Zare, "Load-independent harmonic mitigation in SCR-fed three-phase multiple adjustable speed drive systems with deliberately dispatched firing angles," *IET Power Electron.*, vol. 11, no. 4, pp. 727-734, 2018.
[22] M. Su, C. Luo, X. Hou, W. Yuan, Z. Liu, H. Hua, and J. Guerrero, "A communication-free decentralized control for grid-connected cascaded PV inverters," *Energies*, vol. 11, no. 6, pp. 1375, 2018.
[23] X. Hou, Y. Sun, H. Han, Z. Liu, W. Yuan, and M. Su, "A fully fecentralized control of grid-connected cascaded inverters," *IEEE Trans. Sustain. Energy*, vol. 10, no. 1, pp. 315–317, Jan. 2019.
[24] H. Jafarian, R. Cox, J. H. Enslin, S. Bhowmik, and B. Parkhideh, "Decentralized active and reactive power control for an AC-stacked PV inverter with single member phase compensation," *IEEE Trans. Ind. Appl.*, vol. 54, no. 1, pp. 345-355, Jan.-Feb. 2018.

Yiwei Pan (S'19) received the B.S. degree in automation and M.S. degree in power electronics from Shandong University, Ji'nan, China, in 2015 and 2018, respectively. He is currently working toward the Ph.D. degree at Aalborg University, Aalborg, Denmark.

His current research interests include multilevel converters and distributed power generation.

Ariya Sangwongwanich (S'15−M'19) received the M.Sc. and Ph.D. degree in energy engineering from Aalborg University, Denmark, in 2015 and 2018, respectively. Currently, he is working as a Postdoc Fellow at the Department of Energy Technology, Aalborg University.

He was a Visiting Researcher with RWTH Aachen, Aachen, Germany from September to December 2017. His research interests include control of grid-connected converter, photovoltaic systems, reliability in power electronics and multilevel converters. He has co-authored the book – Advanced in Grid-Connected Photovoltaic Power Conversion Systems. In 2019, he received the Danish Academy of Natural Sciences' Ph.D. prize and the Spar Nord Foundation Research Award for his Ph.D. thesis. Dr. Sangwongwanich also serves as the Chair of the IEEE Student Branch at Aalborg University.

Yongheng Yang (SM'17) received the B.Eng. degree in electrical engineering and automation from Northwestern Polytechnical University, Shaanxi, China, in 2009 and the Ph.D. degree in electrical engineering from Aalborg University, Aalborg, Denmark, in 2014.

He was a postgraduate student with Southeast University, China, from 2009 to 2011. In 2013, he spent three months as a Visiting Scholar at Texas A&M University, USA. Currently, he is an Associate Professor with the Department of Energy Technology, Aalborg University, where he also serves as the Vice Program Leader for the research program on photovoltaic systems. His current research is on the integration of grid-friendly photovoltaic systems with an emphasis on the power electronics converter design, control, and reliability.

Dr. Yang is the Chair of the IEEE Denmark Section. He serves as an Associate Editor for several prestigious journals, including the IEEE TRANSACTIONS ON INDUSTRIAL ELECTRONICS, the IEEE TRANSACTIONS ON POWER ELECTRONICS, and the IEEE Industry Applications Society (IAS) Publications. He is a Subject Editor of the *IET Renewable Power Generation* for Solar Photovoltaic Systems, including the Maximum Power Point Tracking. He was the recipient of the 2018 *IET Renewable Power Generation* Premium Award and was an Outstanding Reviewer for the IEEE TRANSACTIONS ON POWER ELECTRONICS in 2018.

Frede Blaabjerg (S'86–M'88–SM'97–F'03) was with ABB-Scandia, Randers, Denmark, from 1987 to 1988. From 1988 to 1992, he got the PhD degree in Electrical Engineering at Aalborg University in 1995. He became an Assistant Professor in 1992, an Associate Professor in 1996, and a Full Professor of power electronics and drives in 1998. From 2017 he became a Villum Investigator. He is honoris causa at University Politehnica Timisoara (UPT), Romania and Tallinn Technical University (TTU) in Estonia.

His current research interests include power electronics and its applications such as in wind turbines, PV systems, reliability, harmonics and adjustable speed drives. He has published more than 600 journal papers in the fields of power electronics and its applications. He is the co-author of four monographs and editor of ten books in power electronics and its applications.

He has received 32 IEEE Prize Paper Awards, the IEEE PELS Distinguished Service Award in 2009, the EPE-PEMC Council Award in 2010, the IEEE William E. Newell Power Electronics Award 2014, the Villum Kann Rasmussen Research Award 2014, the Global Energy Prize in 2019 and the 2020 IEEE Edison Medal. He was the Editor-in-Chief of the IEEE TRANSACTIONS ON POWER ELECTRONICS from 2006 to 2012. He has been Distinguished Lecturer for the IEEE Power Electronics Society from 2005 to 2007 and for the IEEE Industry Applications Society from 2010 to 2011 as well as 2017 to 2018. In 2019-2020 he serves a President of IEEE Power Electronics Society. He is Vice-President of the Danish Academy of Technical Sciences too.

He is nominated in 2014-2019 by Thomson Reuters to be between the most 250 cited researchers in Engineering in the world.